Int J Adv Manuf Technol (2012) 61:923–933
DOI 10.1007/s00170-011-3770-z

ORIGINAL ARTICLE

Vision inspection system for the identification and classification of defects in MIG welding joints

G. Senthil Kumar · U. Natarajan · S. S. Ananthan

Received: 2 October 2010 / Accepted: 14 November 2011 / Published online: 9 December 2011

Abstract The variety of vision inspection systems for welding defects in the present manufacturing scenario is needed for overcoming certain limitations such as the problem of inaccuracy in the images, non-uniformed illumination, noise and deficient contrast, and confusion in defects if they occur in the same spot at the surface and subsurface. Hence, it is imperative to design a new vision inspection system which will enable to overcome the aforementioned problems in welding. A sophisticated new vision inspection system using machine vision has been developed for this study to identify and classify the surface defects of butt joint as per standard EN25817 in metal inert gas (MIG) welding. In this proposed vision system, images of welding surfaces are captured through a CCD camera. Four frames of sequence of images are obtained using four zones of LEDs using the front light illumination system in this method. From these images, the regions of interest are segmented and the average gray levels of the characteristic features of these images are calculated. The same process can be extended further to four zones (four quadrants) of four types of welded joints. Finally, welded joints can be classified into one of the four predefined ones based on the back-propagation neural network. The proposed system demonstrates an overall accuracy of 95% from the 80 real samples tested.

Keywords Machine vision · Weld classification · Industrial inspection · Back-propagation neural network (BPN)

G. Senthil Kumar (✉)
Department of Mechanical Engineering,
Velammal College of Engineering & Technology,
Madurai 625 009 Tamil Nadu, India
e-mail: senthilgandhi@ymail.com

U. Natarajan
Department of Mechanical Engineering,
A. C. College of Engineering & Technology,
Karaikudi 630 004 Tamil Nadu, India

S. S. Ananthan
Welding Research Institute, Bharat Heavy Electricals Ltd.,
Tiruchirapalli 620014, India

1 Introduction

Over the last four decades, the worldwide manufacturing markets have been facing heavy competition to produce cost-effective higher quality products. This has led to great advances in the technology required for automating production processes, but problems in inspection and quality control are yet to be fully resolved. Due to these gaps in the industry, there arises the necessity for active research in inspection and quality control. Inspection of the quality of weld is performed using various non-destructive tests. Though humans (experts) can do better than machines in many ways in the content of visual inspection and quality control, they get tired quickly and the process becomes slow. Human inspection of weld defects is a hard and difficult task when great numbers of welds are to be counted and inspected. Many inspection tasks are considered time-consuming and boring for humans to perform. It has been reported that human visual inspection is estimated to account for 10% or more of the total labor costs of manufactured products [1]. Moreover, human experts are difficult to find or to maintain their training, and their skills may take time to develop. Machine vision may effectively replace human inspection in such demanding cases. Non-destructive testing (NDT) is a branch of engineering concerned with the methods of detecting defects in objects without altering the object in any way. The reliable detection of weld defects is one of the most important tasks in non-destructive testing. Improvements in these methods are

necessary because the human factor still has great influences on the evaluation. Welding is a major joining process used to fabricate many engineered artifacts and structures such as cars, ships, space shuttles, offshore drilling plate forms, and pipelines [2]. Shafeek et al. [1] introduced a novel automated vision system to detect and assess the welding defects of gas pipelines from radiographic films. This vision system, used to capture images for the radiographic films, can apply various image processing and computer vision algorithms to detect welding defects and calculate necessary information such as length, width, area, and perimeter of the defects. Shafeek et al. [3] developed another vision system which makes use of various image processing and computer vision algorithms applied to capture images of the radiographic films to recognize the defects and to make acceptance decisions according to international standards. This system was capable of identifying and testing the main types of welding defects in gas pipelines welded by shielded metal arc welding. They are used to capture single images for the radiographic films which are used to identify the subsurface defects only.

On the other hand, developments in image processing, computer vision, artificial intelligence, and other related fields have significantly improved the efficiency of visual inspection techniques. It was reported that about 60–90% of all existing machine vision applications were automated visual inspection. A feature is a value describing an object in a numerical form, and the selection of good features is critical to the success of any classification algorithm. Generally, 2D features are computationally simpler than 3Dfeatures [4]. Efficient techniques for solder joint inspection have been described using three layers of ring-shaped light-emitting diodes (LEDs) with different illumination angles; three frames of images were sequentially obtained, the regions segmented, and then the solder joints classified using a fuzzy membership function and neural network classifier [4]. Jagannathan [5] developed a new system for the intelligent machine vision inspection of wave solder joints. A modified intelligent histogram regarding technique was used that divides the gray level histogram of the captured images from a joint into different modes, and the neural networks was employed to identify and classify the defective solder joints. The back-propagation algorithm was employed to train the neural networks. After training, the neural network was employed to successfully identify and classify the defects of the welded joints. They used images captured with light sources of ring-shaped LEDs with different illumination angles in solder joints. In ring-shaped LEDs, illuminations are focused in the center of the image. In welding images, the sizes of beads are not in circular shape and some informations about the welding beads are missed. Poor quality radiographic images have led to the development of various automatic defect detection algorithms that focus on extracting defects using various image segmentation methods [5–7]. Neural networks are used to improve the computational speed of the system for such activities as feature extraction and interpretation [6]. Two-dimensional images taken under controlled conditions of good lighting and low noise is the simplified strategy of industrial vision applications [8]. NDT is particularly important for critical applications where weld failure can be catastrophic, such as in pressure vessels, load-bearing structural members, and power plants [9]. Lashkia [10] proposed fuzzy reasoning to detect low-contrast defects using local image characteristics such as special contrast, special variance, and distance between two contrast regions. As the measurement system is optical, only the surface of the weld was mapped. A digitized radiographic image is often corrupted by non-uniform illumination, noise, and poor contrast [10]. The applied inspection criteria specified in the standards include the measurement of the height and cross-sectional area of the weld together with detection of porosity density and undercuts [7]. Inspection of welds is important not only to ensure the integrity of the welded engineering artifacts but also to improve the fabrication process [11]. Da Silva et al. [12] also concluded that the lack of a high number of samples to increase the reliability of the classification is a common problem in the automatic interpretation of weld radiographs. Radiographic films usually have noise and deficient contrast due to intrinsic factors involved in the inspection technique, such as non-uniform illumination and the limited range of intensities of the image capture device [13]. Liao and Li [14] developed welding flaw detection based on the fitted line profiles of a weld image and successfully detected 93.33% of various defects from linear welds. Wang and Liao [15] used a set of parameters to classify six possible defects and obtained the highest accuracy of 92%. In this work, 108 data sets were used for training while 12 data sets were used for testing. However, the 12 test samples used for classifying six types of defects are considered small and the success rate for individual defect was not reported. Different types of methods that characterize a shape can be viewed from a different context, such as description-based boundaries and region, local and global shape characteristics, statistical or synthetic object description, object reconstruction ability, or incomplete shape recognition ability [16].

The information capture from different viewpoints can reinforce the diagnosis when a single image is insufficient [17]. In tune with the trend, four zones of LEDs with different illumination angles are used to capture the weld joints. In this newly introduced vision system, 2D feature average gray values are extracted from the MIG welding joints and are classified using the back-propagation neural

network as good weld, excess weld, insufficient weld, and no weld. In general, the calibration process is difficult to carry out in industrial environment due to vibrations and random movements that vary with time [17]. Therefore, any calibration process is not followed in this method. This paper is organized as follows: Section 2 represents the overview of the system. The experimentation functions are discussed in Section 3. Preprocessing of digitized image and feature extraction are discussed in Sections 4 and 5. Neural classifier is discussed in Section 6. The test results are presented in Section 7, followed by the conclusions.

2 System overview

The photograph of the overall inspection system is shown in Fig. 1, A RAPID 1 V3.4 machine vision system is used to capture the images. Vision-based inspection systems are a set of new technologies for non-contact inspections and measurements. The instruments integrate a multitude of technologies including digital imaging, electronics, embedded systems, and software. The Rapid-1 V3.4, a vision-based metrology instrument, utilizes these cutting-edge technologies that enable doing precise inspections. Further innovative design and creative developments have led to a wide range of hardware and software capabilities that will enhance our ability not only to inspect manufactured parts but also in our design and development. Rapid-1 is capable of carrying out diverse measurement tasks including all basic 2D measurements, depth, and even threads parameters. Its primary advantage lies in its high-resolution optics combined with precision work stage and power software.

Fig. 1 RAPID 1 machine vision system

The quality of imaging cannot be changed if the hardware is not suitably designed [18]. Four zones of LEDs with different illumination angles and input camera are controlled by the host computer. Figure 2 shows the four zones of LEDs with different illumination angle positions. Full operations including image capturing and inspection software are executed in the host computer. Four frames of images are sequentially captured as four zones of LEDs are turned on, one after the other, as shown in the following figures.

3 Experimentation

The three main functions are carried out in this experimentation. First of all, different types of joints, like acceptable and unacceptable joints in the single V groove butt welding joint in the MIG welding process, have been prepared as per Standard EN 25817. A carbon steel plate (size, 80×20×4 mm) is used as a parent material in this work. The voltage and current maintained during welding are 27 V and 260 Å. ER 70S6 with a 1.2-mm diameter electrode is used in this experiment. Carbon dioxide is supplied during the welding process, and standoff distance is maintained at 15 mm.

The second one is based on the values obtained for the various measurements; acceptance or non-acceptance of the weld will be decided in conformity with the EN 25817 acceptance levels for intermediate service conditions. Figure 3 depicts the different types of acceptable and unacceptable groove weld profiles in butt joint. Figure 3a shows the image of good weld, where h, b, and t denote the reinforcement height, width of the weld, and thickness of the workpiece, respectively. Good weld occurs when the reinforcement height (h) is $h \leq 1$ mm$+0.15b$, maximum of 7 mm, and also the under groove height is $h_1 \leq 0.1t$, maximum of 1 mm. Figure 3b shows excessive reinforcement. When the reinforcement height (h) of the weld lies between 1 and 7 mm, then it is called as excessive reinforcement. Figure 3c shows insufficient weld. When the under groove height (h_1) lies between 0.1 and 1 mm, then it is called

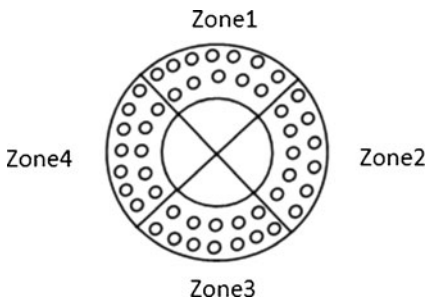

Fig. 2 Four zones of LED illumination

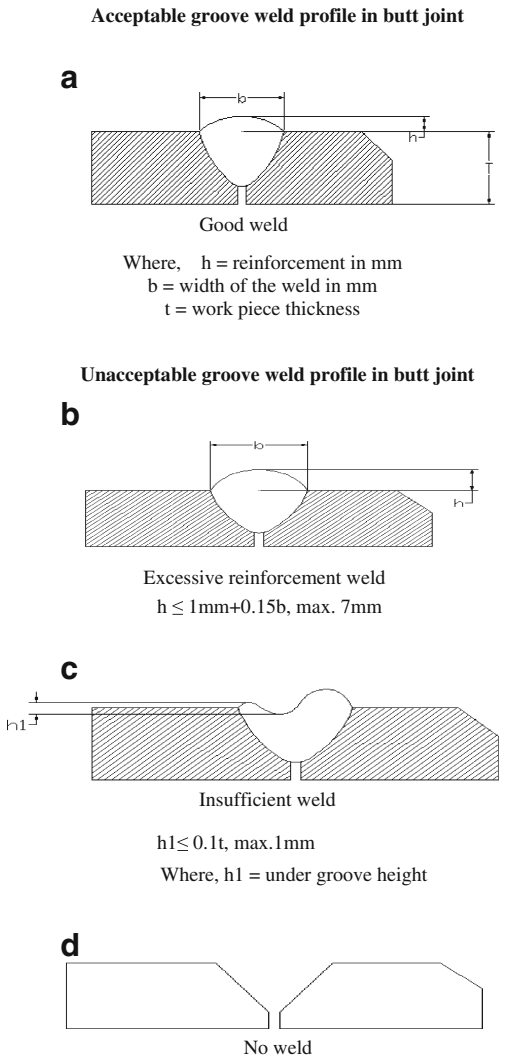

Fig. 3 Different types of acceptable and unacceptable groove weld profiles in butt joint as per EN 25817: Good weld (**a**), excessive reinforcement weld (**b**), insufficient weld (**c**), and no weld (**d**)

insufficient weld. Figure 3d illustrates no weld. When the groove surface is not filled, then it is called no weld.

The types of welding defects to be inspected include defect-free welded joint (good weld), excess weld, insufficient weld, and no weld. Figure 4 shows the images of defect-free welded joint in four zones. Figure 4a–d shows the top left quadrant (zone 1), the top right quadrant (zone 2), the bottom left quadrant (zone 3), and the bottom right quadrant (zone 4) of the image of the defect-free welded joint, respectively. Figure 5 shows the images of excess weld in four zones. In Fig. 5a–d, shown are zones 1, 2, 3, and 4 of the four quadrants of images of excess weld, respectively. Figure 6 shows images of insufficient weld in four zones. Information about zones 1, 2, 3, and 4 of the four quadrants of images of insufficient welds are shown in Fig. 6a–d, respectively. Figure 7 shows the images of no weld in four zones. Figure 7a–d also illustrates information on zones 1, 2, 3, and 4 of the four quadrants of images of no weld. Four zones of LEDs with different illuminations are used to capture four types of weld joints and processed using the RAPID 1 V3.4 machine vision system.

4 Preprocessing

Four frames of images sequentially captured as four zones of LEDs are turned on, one after the other. Image processing seeks to modify and prepare the pixel values of a digitized image to produce more suitable forms for subsequent operations. In this stage, the weld region must be isolated from the rest of the parent metals. Noise on images usually appears as randomly dispersed pixels having different values of intensity in relation to their nearest pixels. Low-pass filters are usually employed to remove the noise and extend the technique of fuzzy k-means clustering followed by the cropping mechanism. The ROI has been identified (Fig. 8).

5 Feature extraction

A feature is a value describing an object in a numerical form; the selection of good features is critical to the success of any classification algorithm. Rather than directly using the raw data, some measures or descriptors are often selected, upon which the classes of the observed objects are determined by a classifier. These measures, commonly called features, form the feature space that is generally of a much lower dimension than the data space. The process of searching for internal structure in data items, that is, for features or properties of the data, is called feature extraction. The process of choosing desirable features from the initial set of candidates is called feature selection. The relevance of extracted features is determined either by trial and error or based on an automatic feature selection procedure [19].

The extraction of desirable features is an extremely difficult task and is very much problem-dependent [9]. In order to distinguish welds from non-welds, features with discriminating capability must be identified [20]. In this process, 2D features are the average gray levels, and the percentages of highlights of I_1, I_2, I_3, and I_4 are extracted from the digitized images of samples. The bitmap images are read and stored into an array variable. Then, true color images are converted into grayscale images. After this selection, a region of interest is cropped for further processing. Finally, average values of pixels in the cropped images are computed as follows [4]:

$$x = \left(x_1, x_2, x_3, x_4\right) \tag{1.1}$$

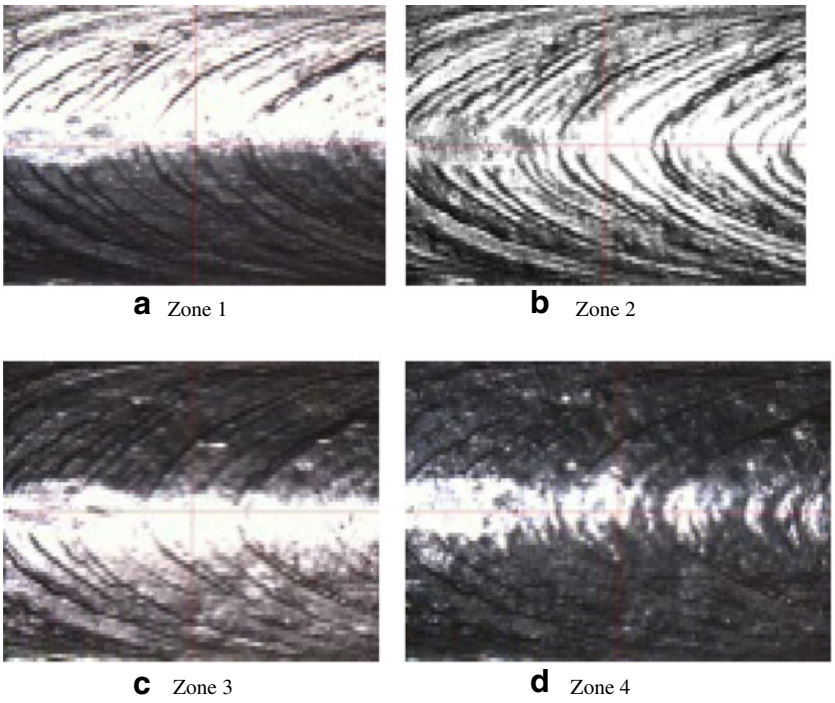

Fig. 4 Four images of good weld: zone 1 (**a**), zone 2 (**b**), zone 3 (**c**), and zone 4 (**d**)

$$x_1 = \frac{1}{N} \sum_{(x,y)\in R} I_1 \quad (x,y) \tag{1.2}$$

$$x_2 = \frac{1}{N} \sum_{(x,y)\in R} I_2 \quad (x,y) \tag{1.3}$$

$$x_3 = \frac{1}{N} \sum_{(x,y)\in R} I_3 \quad (x,y) \tag{1.4}$$

$$x_4 = \frac{1}{N} \sum_{(x,y)\in R} I_4 \quad (x,y) \tag{1.5}$$

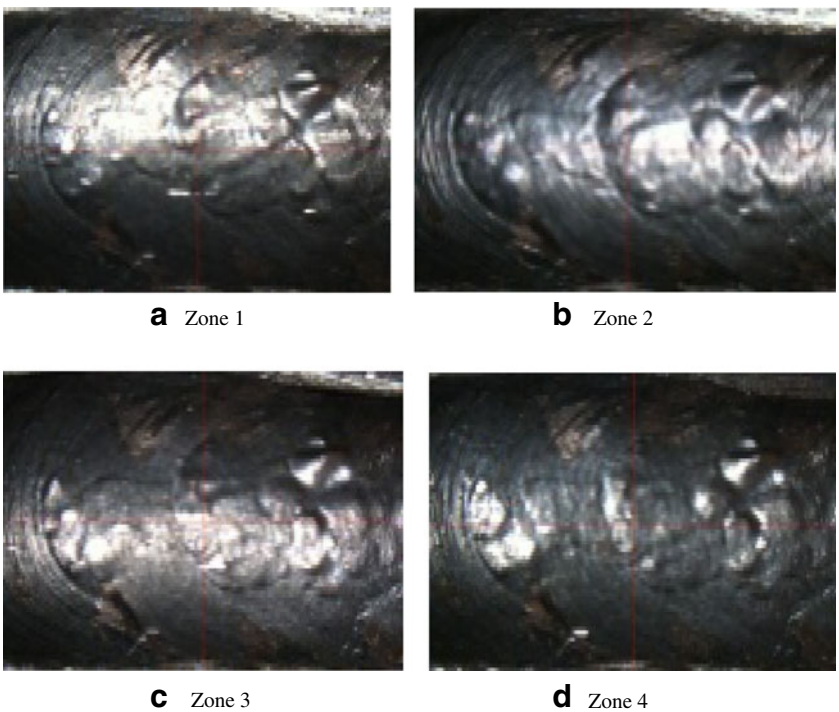

Fig. 5 Four images of excess weld: zone 1 (**a**), zone 2 (**b**), zone 3 (**c**), and zone 4 (**d**)

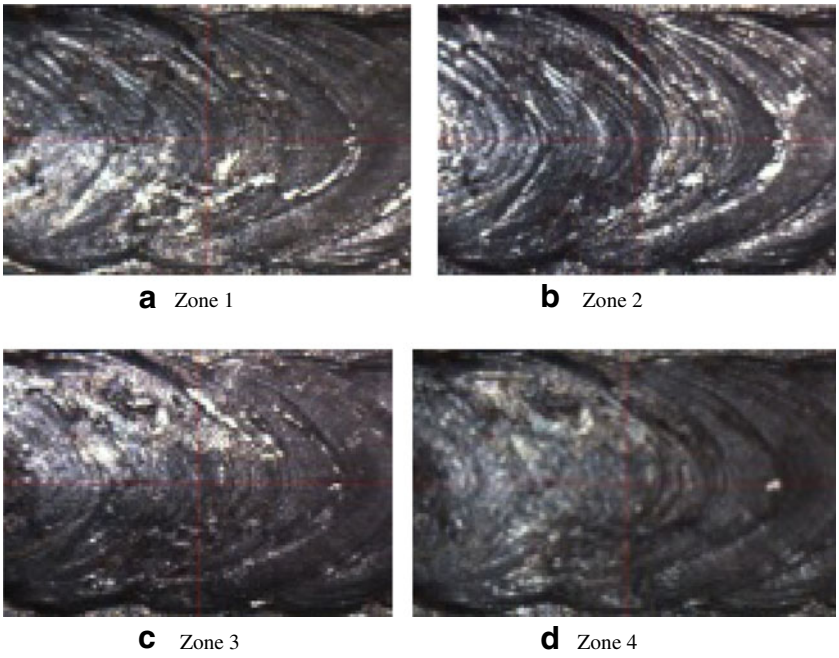

Fig. 6 Four images of insufficient weld: zone 1 (**a**), zone 2 (**b**), zone 3 (**c**), and zone 4 (**d**)

where x is the 2D feature vector, x_1 is the average grayscale value of zone 1 cropped image, x_2 is the average grayscale value of zone 2 cropped image, x_3 is the average grayscale value of zone 3 cropped image, x_4 is the average grayscale value of zone 4 cropped image, $I_i(x, y)$ is the image of the ith layer, R is the welded region, and N is the number of pixels in the welded region.

The average gray values of pixels in the cropped images are calculated and tabulated. In this work, 80 welded image samples are taken into account for the classification process. Table 1 shows the average gray values of 80 samples.

6 BPN classifier

An artificial neural network (ANN) is an information processing paradigm that is inspired by the biological nervous

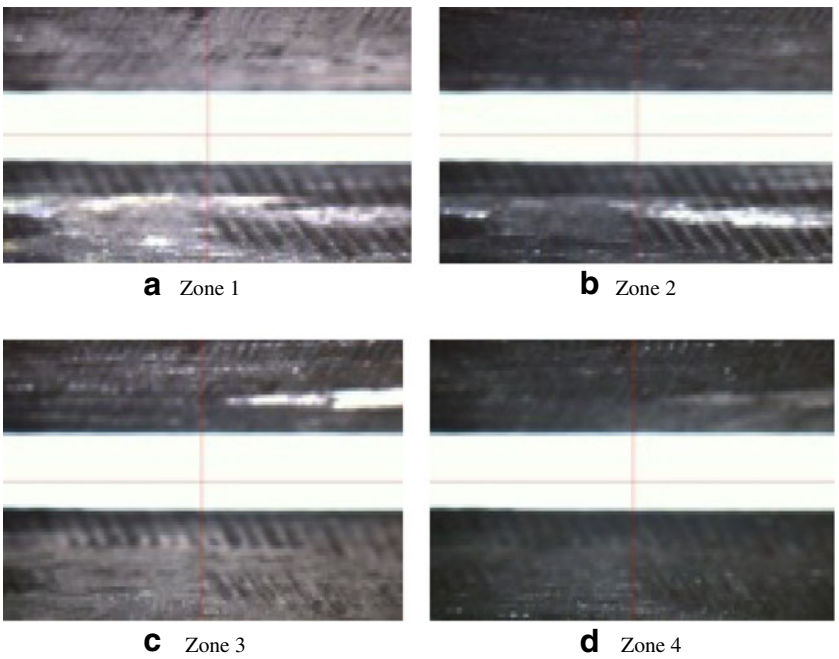

Fig. 7 Four images of no weld: zone 1 (**a**), zone 2 (**b**), zone 3 (**c**), and zone 4 (**d**)

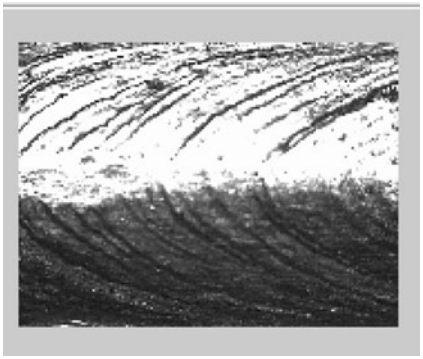

Fig. 8 Grayscale image

systems such as the brain process information. ANN has been successfully employed in similar applications to perform the classification. After feature selection, a back-propagation neural network (BPN) is employed to perform the classification [21]. A block diagram of the back-propagation neural net work is shown in Fig. 9. The back-propagation algorithm minimizes the squares of the differences between the actual output and the desired output unit for all training pairs. The error obtained when a training pair consisting of both input and output is given to the input layer of the network is given by the equation

$$E_p = \frac{1}{2}\sum_i (T_{\mathrm{p}i} - O_{\mathrm{p}i})_2 \tag{2.1}$$

where $T_{\mathrm{p}i}$ is the ith component of the desired output and $O_{\mathrm{p}i}$ is the calculated output of the ith neuron in the output layer.

The overall error of all the patterns is given by,

$$E = \sum E_{\mathrm{p}} \tag{2.2}$$

To obtain a gradient descent in E, the weight W has to be updated

$$W_{ij} = \eta \partial_{pj} O_{pi} \tag{2.3}$$

where η is a constant real number called learning rate which determines the influence of error over weight change, ∂_{pj} is the error due to the pth pattern connected to the jth neuron, and O_{pi} is the ith neuron output when pth is processed by the network.

In the gradient descent, Eq. 2.3, the error value p_j can be computed as follows:

$$\partial_{pj} = O_{pi}\left(1 - O_{pi}\right)\left(T_{pj} - O_{pi}\right) \tag{2.4}$$

For hidden layers,

$$\partial_{pi} = O_{pi}(1 - O_{pi}) \sum \partial_{pj} W_{jk} \tag{2.5}$$

Table 1 Average gray values

Sample no.	Zone 1	Zone 2	Zone 3	Zone 4
1	168.94258	124.0809	144.12504	120.6365
2	169.09755	125.4698	141.8849	119.33363
3	169.06311	128.4559	143.09225	119.28537
4	163.98381	131.1469	143.95048	117.99456
5	163.62224	130.5913	145.11419	118.7787
6	163.01961	131.0774	144.13958	119.61109
7	166.01553	137.015	144.80872	116.7882
8	157.71648	135.4525	138.35014	113.33799
9	161.65939	138.9074	143.87775	114.08594
10	152.72327	133.317	138.48106	110.82875
11	129.23798	102.1362	106.18821	95.954272
12	137.65756	106.2682	113.85412	99.923213
13	158.62903	114.4454	129.91327	109.93604
14	147.98833	110.1571	122.14553	104.45915
15	161.62495	116.4419	131.90612	113.21736
16	159.54158	115.2787	132.35706	113.1691
17	162.38254	117.4315	134.33536	114.77357
18	171.78355	120.7475	141.78308	118.06694
19	172.17956	122.1538	145.4633	120.2384
20	96.145066	90.2785	86.026996	68.992014
21	91.169077	107.987	89.532661	62.031288
22	90.928026	102.1119	81.110336	62.079543
23	82.542881	92.65699	76.135491	57.242019
24	82.077996	92.27504	68.222288	56.228673
25	80.924393	86.63264	64.8039	55.927081
26	77.859597	94.80979	63.989306	53.84007
27	80.61447	104.862	61.065493	52.006395
28	76.120583	92.13615	59.479943	51.487658
29	78.841021	83.54234	60.061797	51.415276
30	101.36211	114.9836	84.208704	57.543611
31	100.65617	98.6119	82.710432	67.640886
32	100.65617	98.6119	82.710432	67.640886
33	109.90221	92.72644	85.69243	84.264595
34	107.23343	81.58051	87.830741	92.70915
35	105.52885	79.4798	104.07899	101.47942
36	100.05354	70.33042	99.045961	102.92706
37	99.089337	73.97629	88.121667	89.729429
38	99.244298	72.58739	88.470779	80.404227
39	93.855078	77.83048	86.652488	79.342626
40	94.474925	73.94156	82.099487	76.628305
41	89.619461	79.63605	86.987053	72.864446
42	89.12014	92.91741	89.547207	60.873178
43	91.909449	95.88618	83.423203	57.14551
44	97.21258	100.0876	80.470298	55.746127
45	93.321322	89.94864	86.536117	64.323382
46	84.075279	98.03898	88.965354	62.224307
47	83.954753	95.55632	91.496416	64.817991
48	80.373419	88.94168	84.645094	61.367788
49	77.859597	89.91391	75.379082	52.766405

Table 1 (continued)

Sample no.	Zone 1	Zone 2	Zone 3	Zone 4
50	71.833312	93.73339	62.34557	43.043103
51	130.71872	152.6748	109.81025	70.138061
52	58.79932	42.95173	52.090408	50.607012
53	69.285055	48.90664	61.472791	59.739195
54	74.20939	45.15661	64.993002	74.480975
55	86.451357	56.00739	72.600733	75.108285
56	94.388835	64.18454	74.59358	76.797196
57	96.007323	68.16027	78.113792	70.668862
58	106.30366	78.88952	79.830259	67.544376
59	110.12605	87.32709	85.837893	71.658081
60	107.38839	93.95909	83.248647	71.851099
61	142.90903	154.1679	122.24736	94.59108
62	143.61497	158.1263	124.21111	84.84365
63	147.00691	173.6125	127.07674	73.383183
64	142.35806	171.8243	117.15614	75.675276
65	139.44823	155.6436	121.91279	88.076709
66	135.50531	166.3902	115.52695	72.406027
67	131.45909	168.1437	114.49416	64.528464
68	132.78488	160.7652	121.92734	77.002278
69	129.15189	156.4943	116.9234	68.412959
70	129.68564	150.2616	116.5161	72.466346
71	70.059863	91.37226	64.658437	44.599314
72	129.28963	116.5287	108.96656	100.7556
73	143.59775	130.1747	117.21433	105.32773
74	147.81615	138.4039	117.22887	101.09339
75	146.28375	142.831	121.25821	101.08132
76	145.25068	151.0082	123.70199	98.946057
77	145.44007	151.4769	126.96037	90.175784
78	144.33813	151.9804	123.58562	89.512283
79	143.28783	153.5082	121.33094	86.641134
80	147.62675	152.6054	120.95273	89.608792

In this work, a BPN classifier is used to classify the weld joints. The back-propagation algorithm was used to train the network. The network was trained by using the average gray values for four zones of images as input variables and the types of weld joint as output variables.

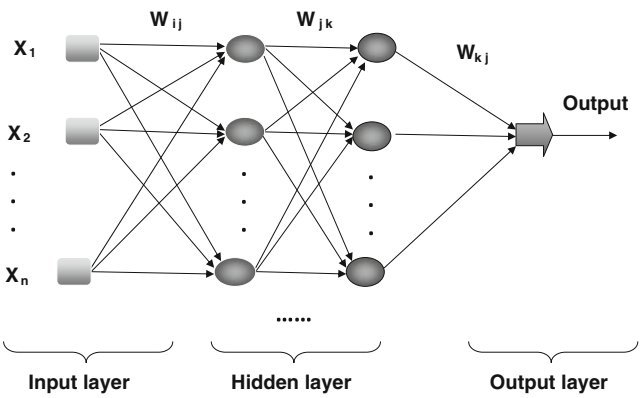

Fig. 9 Block diagram of back-propagation neural net work

In order to improve the performance of the system, normalizing the data is important. It can make the neural network training more efficient due to a significant reduction of the dimensionality of the input data. Normalization is done as follows.

$$x_1 = \frac{x_1}{x_{\max}} \tag{2.6}$$

where x_1 is the average grayscale value of zone 1 image and $x_{\max}$ is the maximum grayscale value of all zone images.

6.1 Input variables

The average gray values of four zones of images for four types of welded joints are used as input variables as follows.

Good weld	Excess weld	Insufficient	No weld
Zone 1	Zone 1	Zone 1	Zone 1
Zone 2	Zone 2	Zone 2	Zone 2
Zone 3	Zone 3	Zone 3	Zone 3
Zone 4	Zone 4	Zone 4	Zone 4

6.2 Output variables

Four types of joints—good weld, excess weld, insufficient, and no weld—are used as output variables. Table 2 shows the inputs and outputs of the training samples.

- Features like the average gray values of four zones for four types of weld joints are the inputs given to the input layer of ANN.
- The weights between the input layer and the hidden layer and the weights between the hidden layer and the output layer are generated randomly for the selected topology 4–5–5–1 of the network.
- The number of training patterns used for training is 80.
- The patterns were normalized.
- The training was done off-line using the computer.

The training function TRAINLM is used in this network. The application of Leven berg–Marquardt to neural network training is the fastest method for training a moderate-sized feed-forward neural network. In many cases, TRAINLM is able to obtain lower mean square errors than any of the other algorithms tested. The number of iterations in this work is 5,000, the learning rate is 0.0001, the hyperbolic tangent function is an activation function, and a three-layer feed-forward BPN is used.

Table 2 Inputs and outputs of the training samples

Type of welding	Sample no.	Zone 1	Zone 2	Zone 3	Zone 4	Output
No weld	1	0.9812	0.7147	0.9908	1	1
	2	0.9821	0.7227	0.9754	0.9892	1
	3	0.9819	0.7399	0.9837	0.9888	1
	4	0.9524	0.7554	0.9896	0.9781	1
	5	0.9503	0.7522	0.9976	0.9846	1
	6	0.9468	0.755	0.9909	0.9915	1
	7	0.9642	0.7892	0.9955	0.9681	1
	8	0.916	0.7802	0.9511	0.9395	1
	9	0.9389	0.8001	0.9891	0.9457	1
	10	0.887	0.7679	0.952	0.9187	1
	11	0.7506	0.5883	0.73	0.7954	1
	12	0.7995	0.6121	0.7827	0.8283	1
	13	0.9213	0.6592	0.8931	0.9113	1
	14	0.8595	0.6345	0.8397	0.8659	1
	15	0.9387	0.6707	0.9068	0.9385	1
	16	0.9266	0.664	0.9099	0.9381	1
	17	0.9431	0.6764	0.9235	0.9514	1
	18	0.9977	0.6955	0.9747	0.9787	1
	19	1	0.7036	1	0.9967	1
	20	0.5584	0.52	0.5914	0.5719	0.75
Insufficient weld	21	0.5295	0.622	0.6155	0.5142	0.75
	22	0.5281	0.58816	0.5576	0.5146	0.75
	23	0.4794	0.5337	0.5234	0.4745	0.75
	24	0.4767	0.5315	0.469	0.4661	0.75
	25	0.47	0.499	0.4455	0.4636	0.75
	26	0.4522	0.5461	0.4399	0.4463	0.75
	27	0.4682	0.604	0.4198	0.4311	0.75
	28	0.4421	0.5307	0.4089	0.4268	0.75
	29	0.4579	0.4812	0.4129	0.4262	0.75
	30	0.5887	0.6623	0.5789	0.477	0.75
	31	0.5846	0.568	0.5686	0.5607	0.75
	32	0.5846	0.568	0.5686	0.5607	0.75
	33	0.6383	0.5341	0.5891	0.6985	0.75
	34	0.6228	0.4699	0.6038	0.7685	0.75
	35	0.6129	0.4578	0.7155	0.8412	0.75
	36	0.5811	0.4051	0.6809	0.8532	0.75
	37	0.5755	0.4261	0.6058	0.7438	0.75
	38	0.5764	0.4181	0.6082	0.6665	0.75
	39	0.5451	0.4483	0.5957	0.6577	0.75
	40	0.5487	0.4259	0.5644	0.6352	0.75
Excess weld	41	0.5176	0.5352	0.6156	0.5046	0.5
	42	0.5338	0.5523	0.5735	0.4737	0.5
	43	0.5646	0.5765	0.5532	0.4621	0.5
	44	0.542	0.5181	0.5949	0.5332	0.5
	45	0.4883	0.5647	0.6116	0.5158	0.5
	46	0.4876	0.5504	0.629	0.5373	0.5
	47	0.4668	0.5123	0.5819	0.5087	0.5
	48	0.4522	0.5179	0.5182	0.4374	0.5
	49	0.4172	0.5399	0.4286	0.3568	0.5
	50	0.4069	0.5263	0.4445	0.3697	0.5
	51	0.3415	0.2474	0.3581	0.4195	0.5
	52	0.4024	0.2817	0.4226	0.4952	0.5
	53	0.431	0.2601	0.4468	0.6174	0.5
	54	0.5021	0.3226	0.4991	0.6226	0.5
	55	0.5482	0.3697	0.5128	0.6366	0.5
	56	0.5576	0.3926	0.537	0.5858	0.5
	57	0.6174	0.4544	0.5488	0.5599	0.5
	58	0.6396	0.503	0.5901	0.594	0.5
	59	0.6237	0.5412	0.5723	0.5956	0.5
	60	0.5205	0.4587	0.598	0.604	0.5
Good weld	61	0.8341	0.9108	0.8539	0.7033	0.25
	62	0.8538	1	0.8736	0.6083	0.25
	63	0.8268	0.9897	0.8054	0.6273	0.25
	64	0.8099	0.8965	0.8381	0.7301	0.25
	65	0.787	0.9584	0.7942	0.6002	0.25
	66	0.7635	0.9685	0.7871	0.5349	0.25
	67	0.7712	0.926	0.8382	0.6383	0.25
	68	0.7501	0.9014	0.8038	0.5671	0.25
	69	0.7532	0.8655	0.801	0.6007	0.25
	70	0.7592	0.8794	0.7549	0.5814	0.25
	71	0.7509	0.6712	0.7491	0.8352	0.25
	72	0.834	0.7498	0.8058	0.8731	0.25
	73	0.8585	0.7972	0.8059	0.838	0.25
	74	0.8496	0.8227	0.8336	0.8379	0.25
	75	0.8436	0.8698	0.8504	0.8202	0.25
	76	0.8447	0.8725	0.8728	0.7475	0.25
	77	0.8383	0.8754	0.8496	0.742	0.25
	78	0.8322	0.8842	0.8341	0.7182	0.25
	79	0.8574	0.879	0.8315	0.7428	0.25
	80	0.83	0.888	0.8404	0.7841	0.25

7 Results and discussion

In this work, the 80 weld joint samples are used for training and testing, respectively. In each set, 20 images are used for each type, giving a total of 80 images for one good and three defect

Table 3 Training and test data of the four types of weld

Sample no.	Type of weld	Training data	Test data
1	Good	20	20
2	Excess weld	20	20
3	Insufficient weld	20	20
4	No weld	20	20
	Total	80	80

Table 4 Classification performance of different types of welding images

Sample no.	Class	Number	Result			
			Correct	Incorrect	Correct (%)	Incorrect (%)
1	Good weld	20	19	1	95	5
2	Excess weld	20	19	1	95	5
3	Insufficient weld	20	20	0	100	0
4	No weld	20	18	2	90	10
	Total	80	76	4	95	5

types training. For testing of the sample, 80 images are used in the BPN network. The training data fed into the neural network are the average gray values of four images for four zones as input variables and the type of weld joint as the output variable. Table 3 shows the training and test data of the four types of weld: good, excess, insufficient, and no weld.

Networks with different topologies have been tried. It is found that a 4–5–5–1 architecture offers a more accurate prediction than any other network structure. The average training error depends upon the iteration number. The performance of the trained BPN that can be reiterated using a set of unseen patterns is known as testing or validation. The second group of data obtained is used for validation. The accuracy of the BPN is determined by means of recognition rate. The recognition rate is mostly dependent on the number of hidden neurons and the learning rate used in the network. The recognition rate is defined as follows:

$$\text{Recognition rate} = \frac{\text{Number of unseen patterns correctly classified}}{\text{Total number of unseen patterns}} \times 100$$

The network was trained at 0.0001 allowable errors; it can be seen that the error coverage was 7.8222e−005. The performance of the proposed classifier has been evaluated in terms of the recognition rate and the execution time. The classification performance of an individual defect type is shown in Table 4. For individual comparison, it was found that the accuracy varies with the type of defect. The highest accuracy is 100% for insufficient weld and the lowest is for no weld (90%). The overall accuracy is 95%. As a matter of fact, a 2D feature shows a significant difference in the comparison test. The performance of a BPN network using 80 samples is shown in Fig. 10.

8 Conclusion

The technique used in this method for welding joint inspections using 2D feature extraction of images by a machine vision system has been developed and verified with real welding defects. Four zones of LEDs are used for the efficient extraction of shape information which is used to characterize weld defects, and it can be classified into one of the predefined ones based on the back-propagation neural network. The classification of real defects using this method provides the highest overall accuracy of 95%. This same method was used in single image captured by a front light illumination system and which was performed only in a 92.5% accuracy level. Thus, the proposed method overcomes the problem of inaccuracy in the images, non-uniformed illumination, noise and deficient contrast, and confusion in defects

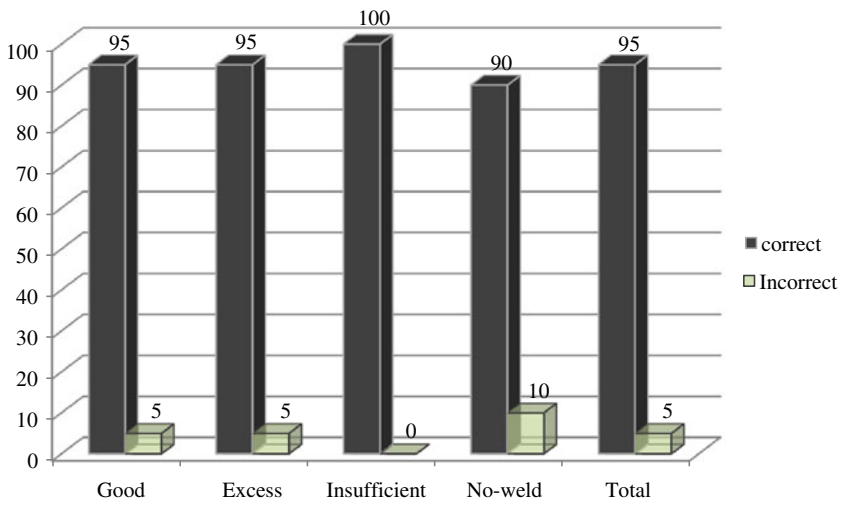

Fig. 10 Classification performance of BPN network using 80 samples

if they occur in the same spot at the surface and the subsurface in a certain level. Future work is to be extended to extract 3D features through the distribution of illuminations in different tilt angles. The estimation of tilt angle at each pixel position (x,y) gives a 3D shape information of the welded joints, and the reflected slant angle measures the angle between the x-axis and projection of the xy plane. This 3D feature extraction approach will increase the classification accuracy. It can be used in computer-aided inspection of welding defects in manufacturing systems. This vision-based inspection system could be further used for the classification of images with different joints in the welding process.

References

1. Shafeek HI, Gadelmawla ES, Abdel-Shafy AA, Elewa IM (2004) Assessment of welding defects for gas pipeline radiographs using computer vision. NDT&E International 37:291–299
2. Warren Liao T (2009) Improving the accuracy of computer-aided radiographic weld inspection by feature selection. NDT&E International 42:229–239
3. Shafeek HI, Gadelmawla ES, Abdel-Shafy AA, Elewa IM (2004) Automatic inspection of gas pipeline welding defects using an expert vision system. NDT&E International 37:301–307
4. Kim T-H, Cho T-H, Moon YS, Park SH (1999) Visual inspection system for the classification of solder joints. Pattern Recognition 32:565–575
5. Jagannathan S (1997) Automatic inspection of wave soldered joints using neural networks. J Manuf Syst 16(6):389–398
6. Jagannathan S (1992) Intelligent inspection of wave soldered joints—technical report. Journal of Manufacturing Systems 11(2):137–143
7. Gauss M, Buerkle A, Laengle T, Woern H, Stelter J, Ruhmkorf S, Middelmann R (2003) Adaptive robot based visual inspection of complex parts. ISR2003
8. Malamas EN, Petrakis EGM, Zervakis M, Petit L (2003) A survey on industrial vision systems, applications and tools. Image and Computing 21:171–188
9. Liao TW, Li D-M, Li Y-M (1999) Detection of welding flaws from radiographic images with fuzzy clustering methods. Fuzzy Set Syst 108:145–158
10. Lashkia V (2001) Defect detection in X-ray images using fuzzy reasoning. Image and Vision Computing 19:261–269
11. Liao TW (2003) Classification of welding flaw types with fuzzy expert systems. Expert Systems with Application 25:101–111
12. da Silva RR, Caloba LP, Siqueira MHS, Rebello JMA (2004) Pattern recognition of weld defects detected by radiographic test. NDT&E International 37:461–470
13. Vilar R, Zapata J, Ruiz R (2009) An automatic system of classification of weld defects in radiographic images. NDT&E International 42:467–476
14. Liao TW, Li YM (1998) An automated radiographic NDT system, for weld inspection: Part II—Flaw detection. NDT&E International 31(3):183–192
15. Wang G, Liao TW (2002) Automatic identification of different types of welding defects in radiographic images. NDT &E International 35:519–528
16. Sonka M, Hilavac H, Boyle R (1998) Image processing, analysis and machine vision, 2nd edn. PWS Publishing, Pacific Grove
17. Carrasco M, Merry D (2011) Automatic multiple view inspection using geometrical tracking and feature analysis in aluminum wheels. Machine Vision and Applications 22:157–170
18. Wang Y, Sun Y, Lv P, Wang H (2008) Detection of line weld defects based on multiple thresholds and support vector machine. NDT&E International 41:517–524
19. Waren Liao T, Li Damin, Li Yueming (2000) Extraction of welds from radiographic images using fuzzy classifiers. Information Sciences 126:21–40
20. Waren Liao T, Tang K (1997) Automated extraction of welds from digitized radiographic images based on MLP neural networks. Appl Artif Intell 11:197–218
21. Garcia-Allende PB, Mirapeix J, Conde OM, Cobo A, Lopez-Higuera JM (2009) Spectral processing technique based on feature selection and artificial neural networks for arc-welding quality monitoring. NDT&E International 42:56–63